



CHORUS

This is the accepted manuscript made available via CHORUS. The article has been published as:

Shear-induced mechanical failure of β -Ga₂O₃ from quantum mechanics simulations

Qi An and Guodong Li

Phys. Rev. B **96**, 144113 — Published 30 October 2017

DOI: [10.1103/PhysRevB.96.144113](https://doi.org/10.1103/PhysRevB.96.144113)

Shear Induced Mechanical Failure of β -Ga₂O₃ from Quantum Mechanics Simulations

Qi An^{1,*} and Guodong Li²

Department of Chemical and Materials Engineering, University of Nevada, Reno,

Reno, Nevada, 89577, United States

State Key Laboratory of Advanced Technology for Materials Synthesis and Processing, Wuhan

University of Technology, Wuhan 430070, China.

*Corresponding author E-mail: qia@unr.edu

Abstract: Monoclinic gallium oxide (β -Ga₂O₃) has important applications in power devices and deep UV optoelectronic devices because of such novel properties as wide-bandgap, high breakdown electric field, and wide range of n-type doping conductivity. However, the intrinsic failure mechanisms of β -Ga₂O₃ remain unknown, which limits the fabrication and packaging of β -Ga₂O₃ based electronic devices. Here we used density functional theory (DFT) at the Perdew–Burke–Ernzerhof (PBE) level to examine the shear induced failure mechanisms of β -Ga₂O₃ along various plausible slip systems. We found that the (001)/<010> slip system has the lowest ideal shear strength of 3.8 GPa among five plausible slip systems, suggesting that (001)/<010> is the most plausible activated slip system. This slip leads to an intrinsic failure mechanism arising from breaking the longest Ga–O bond between octahedral Ga and fourfold coordinated O. Then we identified the same failure mechanism of β -Ga₂O₃ under biaxial shear deformation that mimics indentation stress conditions. Finally, the general stacking fault energy (SFE) surface is calculated for (001) surface from which we concluded that there is no intrinsic stacking fault structure for β -Ga₂O₃. The deformation modes and SFE calculations are essential to understand the intrinsic mechanical processes of this novel semiconductor material, which provides insightful guidance for designing high-performance semiconductor devices.

1. Introduction

Gallium oxide (Ga_2O_3) belongs to a family of transparent conducting oxides (TCOs) that are widely used in such technological applications as laser lithography, display panels, and thin-film transparent field-effect transistors [1–4]. Several crystalline phases for Ga_2O_3 have been discovered so far, including α , β , γ , ϵ , and δ polymorphs [5]. The most stable phase at ambient conditions is monoclinic gallium oxide ($\beta\text{-Ga}_2\text{O}_3$) that exhibits such novel properties as wide-bandgap (~ 4.8 eV) [6,7], high breakdown electric field (8 MV/cm) [8], and wide range of n-type doping conductivity [9,10]. The combination of these properties makes it very useful in power devices applications, in high temperature chemical gas sensors, and in deep UV optoelectronic devices [11–13]. One essential basic parameter for power devices applications is the Baliga's figure of merit (FOM) [14] which is proportional to the cube of the break down field, but only linearly proportional to the electron mobility and dielectric constant. The Baliga's FOM of $\beta\text{-Ga}_2\text{O}_3$ is at least four times larger than those of 4H-SiC or GaN [11], suggesting that $\beta\text{-Ga}_2\text{O}_3$ is a promising material for power devices.

Recent advance in the fabrication processes of semiconductor devices has resulted in large and high-quality single crystals $\beta\text{-Ga}_2\text{O}_3$ (≥ 2 inch in diameter), synthesis through melt growth methods such as Czochralski [15], floating-zone [16], and edge-defined film-fed growth [17]. Consequently, high-quality $\beta\text{-Ga}_2\text{O}_3$ homoepitaxial films can be grown by molecular beam epitaxy [18] and halide vapor phase epitaxy [19]. Applying these fabrication techniques, novel electronic devices have been synthesized such as the $\beta\text{-Ga}_2\text{O}_3$ based high voltage (>750 V)

metal-semiconductor field-effect transistors [20] and the β -Ga₂O₃ Schottky barrier diodes [21]. These advances on the β -Ga₂O₃ offer a growth platform for power devices and optoelectronic applications in the near future.

Although the electronic and optical properties of β -Ga₂O₃ have been and still are the subject of extensive investigation; the mechanical properties of β -Ga₂O₃ often dictate fundamental limits on the fabrication and packaging of β -Ga₂O₃ based electronic devices. In particular, thermal stress during growth may affect the structural quality, such as dislocation formation, twinning, and cracking [22]. In addition, the thermal stress and residual stress in heterogeneous structures play an essential role in the degradation and mechanical failure of the β -Ga₂O₃ based devices at extreme working environments such as high temperature, high pressure, high strain rate deformation, and high strength electric field. However, the understanding on the mechanical properties of β -Ga₂O₃ is very limited. Particularly, the intrinsic deformation and failure mechanisms of β -Ga₂O₃ remain unknown.

In order to obtain the atomistic understanding of the failure mechanisms of β -Ga₂O₃, we carried out density functional theory (DFT) simulations at PBE level to examine the deformation and failure modes, and other mechanical properties of β -Ga₂O₃. We first applied pure shear deformation on crystalline β -Ga₂O₃ to obtain the ideal shear strength and intrinsic failure modes. Then, we examined the deformation modes and failure mechanisms under biaxial shear deformation that mimics the experimental indentation stress conditions. Finally, the general stacking fault (GSF) energy surface was computed to understand the dislocation properties of

β -Ga₂O₃.

2. Methodology

All quantum mechanics (QM) simulations were performed using the Vienna Ab-initio Simulation Package (VASP) plane wave periodic code [23–26]. The projector augmented wave (PAW) method and the Perdew–Burke–Ernzerhof (PBE) functional were applied. The plane-wave cutoff energy was set to 600 eV which gives excellent convergence on energy, force, stress, and geometries. The electron partial occupancies were determined using the tetrahedron method with Blöchl corrections [27]. The $4s^24p^1$ electrons of Ga and $2s^22p^4$ electrons of O were treated as valence states to generate the PAW potentials. The energy error for terminating electronic self-consistent field (SCF) and the force criterion for the geometry optimization were set equal to 10^{-6} eV and 10^{-3} eV/Å, respectively. Brillouin-zone integration was performed on Γ -centered symmetry reduced Monkhorst-Pack meshes with a fine resolution of $2\pi \times 1/40$ Å⁻¹ for all calculations.

To predict the mechanical properties, the elastic constant C_{ij} were first derived from the stress–strain relationship as a function of various cell distortions from the equilibrium lattice configuration [28]. Then, the stiffness constant S_{ij} were derived from the matrix inversion of the elastic constant C_{ij} , which is $S_{ij} = (C_{ij})^{-1}$. Finally, the Voigt–Reuss–Hill (VRH) approximation [29] is applied to calculate the isotropic polycrystalline elastic moduli from the corresponding single-crystal elastic and stiffness constants.

To determine the ideal shear strength and the deformation mechanism under pure shear

deformation, we imposed the strain for a particular shear plane while allowing full structure relaxation for the other five strain components [30]. To mimic the complex stress conditions under indentation experiments, we applied biaxial shear deformation where the ratio of the compressive pressure beneath the indenter normal to the chosen shear plane has a fixed fraction of the tangential shear while the other four strain components are relaxed [31]. The normal stress (σ_{zz}) and shear stress (σ_{xz}) will be constrained to the relationship $\sigma_{zz} = \sigma_{zx} \tan \Phi$, where $\Phi = 68^\circ$ for a Vickers indenter. This leads to $\sigma_{zz} = 2.48 \times \sigma_{zx}$, suggesting highly compressive stress under indentation conditions. The residual stresses after relaxing were less than 0.2 GPa for both pure shear and biaxial shear deformation. A double unit cell along b or c axis is applied for both pure shear deformation and indentation stress conditions.

An intrinsic stacking fault (ISF) can be produced via a sliding process. Sliding of one part of a β -Ga₂O₃ crystal over another across a (001) plane in two directions of [100] and [010] yields a general stacking fault structure [32]. The extra energy per unit area of the stacking fault (GSF energy or γ -surface) is then calculated as a function of fault translation vector \mathbf{d} . The lattice vectors and the atoms coordination were not allowed to relax in the γ -surface calculations so that the unrelaxed γ -surface is derived.

3. Results and Discussion

3.1 Crystal structure, elastic modulus and hardness

The β -Ga₂O₃ has monoclinic unit cell with $C2/m$ symmetry. In the unit cell, there are two nonequivalent Ga atoms occupying the tetrahedral (Ga_I) and octahedral (Ga_{II}) sites, and there are

three nonequivalent O atoms with two threefold (O_I and O_{II}) and one fourfold (O_{III}) coordinated sites, as shown in Fig. 1. For this monoclinic structure, PBE gives equilibrium lattice parameters $a = 12.50 \text{ \AA}$, $b = 3.10 \text{ \AA}$, $c = 5.92 \text{ \AA}$, and $\beta = 103.7^\circ$, leading to a density of 5.59 g/cm^3 . Our results agree very well with previous experimental lattice parameters of $a = 12.23 \text{ \AA}$, $b = 3.04 \text{ \AA}$, $c = 5.80 \text{ \AA}$, and $\beta = 103.7^\circ$ [33]. The bond lengths in distorted GaO_4 tetrahedron are 1.879 \AA ($\text{Ga}_I\text{-O}_I$ and $\text{Ga}_I\text{-O}_{II}$) and 1.916 \AA ($\text{Ga}_I\text{-O}_{III}$). The bond lengths in the distorted GaO_6 octahedron are 1.982 \AA ($\text{Ga}_{II}\text{-O}_I$), 1.977 \AA ($\text{Ga}_{II}\text{-O}_{II}$), 2.046 \AA ($\text{Ga}_{II}\text{-O}_{III}(2)$), and 2.101 \AA ($\text{Ga}_{II}\text{-O}_{III}$). Therefore, the longest Ga–O bond in $\beta\text{-Ga}_2\text{O}_3$ corresponds to the $\text{Ga}_{II}\text{-O}_{III}$ bond, suggesting it is the weakest bond. While the shortest Ga–O bond corresponds to $\text{Ga}_I\text{-O}_I$ bond, suggesting it is the strongest bond. The Ga–O bond lengths from DFT simulations agree very well with previous experimental measurements [33].

To examine the mechanical properties, we used QM to predict the elastic moduli of $\beta\text{-Ga}_2\text{O}_3$ using Voigt–Reuss–Hill averaging [29]. The predicted $B = 162.9 \text{ GPa}$ and $G = 69.8 \text{ GPa}$ which are consistent with the previous prediction [34]. The ductility of metals and alloys can be assessed using the empirical Pugh’s criterion that the ratio of the bulk modulus to the shear modulus (B/G) of ductile materials should be larger than 1.75 [35]. However, the Pugh’s criterion for semiconductors and ceramics has not been established yet. For $\beta\text{-Ga}_2\text{O}_3$, the $B/G = 2.33$ which is larger than 1.75, but future studies are required to determine whether the $\beta\text{-Ga}_2\text{O}_3$ is ductile or brittle.

Generally, the materials strength is judged by indentation hardness, which measures the

resistance of materials to deformation at a constant compression load. The calculated Vickers hardness (H_v) for polycrystalline β -Ga₂O₃ based on G/B [36] leads to $H_v = 5.9$ GPa, which is comparable to Zr-based bulk metallic glasses [36]. We also predicted the Knoop hardness of β -Ga₂O₃ by applying the method that takes into account the important chemical effects related to the strength of covalent bonding, degree of ionicity and directionality, and topology of the crystal structure [37]. The predicted Knoop hardness is 9.2 GPa which is larger than the Vickers hardness of 5.9 GPa.

3.2 Deformation and failure mechanism under ideal shear deformation

The ideal strength of a material is the maximum stress above which elastic strain is unstable [38]. This is a fundamental mechanical property directly related to the nature of chemical bonding in the crystal [39,40]. The value of the ideal strength depends on the type of deformation: tension, compression, or shear, and the direction of the applied strain. Theoretically, the value of the ideal shear strength is related to the stress necessary for the nucleation of a dislocation in metals [41], and for the amorphous shear band formation in superhard materials [42,43] and thermoelectric materials [44]. Here we applied the pure shear deformation on β -Ga₂O₃ to determine its ideal shear strength and intrinsic failure mechanism. Previous studies suggested that shear failure can also occur due to simple uniaxial tensile loading [45]. The failure mode can be predicted in the future through an analytical model based on second-order and third-order elastic constants [45–47].

To determine the most plausible activated slip systems under realistic conditions, we applied

pure shear deformation along various slip systems of (001)/<010>, (001)/<100>, (010)/<100>, (100)/<001> and (100)/<010>. These low crystallographic planes (100), (010) and (001) are selected because the β -Ga₂O₃ is easily cleaved along (100) and (001) planes [43]. The shear-stress–shear-strain relationships displayed in Fig. 2(a) show that the barrier stress for ideal shear deformation along (001)/<010> is 3.8 GPa, which is much lower than those for shearing along (001)/<100> (12.8 GPa), (010)/<100> (13.3 GPa), (100)/<001> (19.5 GPa), and (100)/<010> (13.3 GPa), respectively. Therefore, (001)/<010> is the least stress shear slip system for β -Ga₂O₃.

The details of deformation and failure process for shearing along (001)/<010> are displayed in Fig. 2(b)–(e). Fig. 2(b) shows the intact structure. As the system is sheared to 0.123 strain that corresponds to the maximum shear stress of 3.8 GPa, the Ga₆–O₆ bond (Ga_{II}–O_{III} type) is stretched from 2.101 to 2.338 Å. But the structure does not deconstruct, as shown in Fig. 2(c). Then this Ga₆–O₆ bond breaks with the bond length dramatically increasing from 2.338 to 2.643 Å as the shear strain increases to 0.144, leading to the structural failure (Fig. 2(d)) with the shear stress decreasing from 3.8 to 1.6 GPa. Finally, the shear stress further decreases to ~0 GPa as the shear strain increases 0.166. The Ga₆···O₆ distance now increases to 2.943 Å, as shown in Fig. 2(e). Therefore, the deconstruction of β -Ga₂O₃ along (001)/<010> slip system arises from breaking the Ga₆–O₆ bond which belongs to Ga_{II}–O_{III} bond, the weakest bond in β -Ga₂O₃.

The high-resolution electron microscope observations of the β -Ga₂O₃ subjected to nanoindentation revealed the formation of the stacking faults along the (200) planes, the twinning

structures with (201) plane as twin boundary, and the dislocations on (101) lattice planes [48]. The above deformation mechanism of Ga6-O6 bond breaking may provide a deformation path accommodating the stress built-up as shear strain increases. While future studies may be required to examine the other plausible dislocation nucleation paths.

We also examined the details of failure process along (001)/<100> slip system, as displayed in Fig. 3(a)-(c). The (001)/<100> slip system has the second lowest ideal shear strength and may also be activated under specific loading conditions. Fig. 3(a) displays the intact structure before shear. As the system is sheared to 0.254 strain before failure (Fig. 3(b)), the Ga8-O5 bond does not break, with the bond length increasing from 2.046 to 2.244 Å. However, this Ga8-O5 bond breaks as the shear strain increases to 0.276 with the Ga···O distance dramatically increasing to 3.777 Å. This results in the cleavage along (100) plane and mechanical failure of β -Ga₂O₃, as shown in Fig. 3(c). This failure process arises from breaking the second longest Ga-O bond which belongs to Ga_{II}-O_{III}(2) bond in β -Ga₂O₃. It is worth to notice that the cleave plane is (100) if the β -Ga₂O₃ is sheared along (001)/<100>. Our simulation results suggested that the (100) cleavage happens when the second longest bond Ga_{II}-O_{III}(2) breaks. This may provide a plausible mechanism explaining the experimental observed cleavage along (100) plane [49].

Our current study sheds light on the intrinsic mechanics of ideal crystal β -Ga₂O₃. The strength of realistic β -Ga₂O₃ should be much lower than the values from first-principles calculations because of the defects such as grain boundaries (GBs) and vacancies. In addition, the GBs and vacancies may be the nucleation sites for the dislocations and stacking faults

observed in experiments [48,50]. However, understanding how an ideal crystal fails will allow future work to understand the role that grain boundaries and vacancies play in real materials.

3.3 Deformation and failure mechanism under indentation stress conditions

Micro- and nano-indentation experiments provide the experimental means to validate the predicted properties of strength and hardness from theory [51]. In addition, recent advances in nano-indentation have provided information about such new phenomena as local phase transformation, dissipative kink band formation, and strength enhancement [52–55]. This has led to theoretical studies to elucidate the atomistic mechanics and mechanisms of materials deformation under indentation [56,57]. Consequently, examining the structural changes and deformation mechanisms under indentation conditions is essential to predict and understand the indentation experiments. Therefore, it is important to identify the deformation and failure mechanisms of β -Ga₂O₃ under indentation stress conditions.

We applied biaxial shear deformation on β -Ga₂O₃ to predict its mechanical behaviors in the indentation experiments. Considering low ideal shear strength, we selected several possible slip systems of (001)/<010>, (001)/<100>, (010)/<100>, and (100)/<010> for biaxial shear deformation. The shear-stress–shear-strain relationship shown in Fig. 4(a) indicates that the barrier shear stress for biaxial shear deformation along (001)/<010> is 3.5 GPa which is 82.9%, 111.4% and 228.6% lower than those of shearing along (100)/<010> (6.4 GPa), (010)/<100> (7.4 GPa), and (001)/<100> (11.5 GPa) slip systems, respectively. It is worth to notice there is a shear stress drop before reaching maximum shear stress for (100)/<010> slip. The detailed structural

analyses indicate that the structure does not deconstruct at this stress drop, which will be discussed below. Therefore, the least stress shear slip system is still (001)/<010> under indentation stress conditions, while is the same as the pure shear deformation. This suggests that the (001)/<010> slip system is most plausible to be activated at realistic conditions.

The details failure mechanisms shearing along (001)/<010> are displayed in Fig. 4(b)-(d). With the shear strain increases to 0.123 which corresponds to maximum shear stress of 3.5 GPa, the Ga6–O6 bond is stretched from 2.101 to 2.231 Å. But the structure is not deconstructed, as shown in Fig. 4(b). The increase of Ga6–O6 bond length is smaller than that in the pure shear deformation because of the compressive stress. As the shear strain increases to 0.144, the Ga6–O6 bond slightly decreases from 2.231 to 2.291 Å. This slightly decreases the shear stress by 0.1 GPa and the structure is not deconstructed, as shown in Fig. 4(c). After passing the critical strain, the Ga6–O6 bond breaks at 0.166 strain, leading to the failure (Fig. 4(d)). This failure mechanism is the same as the pure shear deformation, suggesting that the critical failure mechanism can be validated by indentation experiments.

The details of the deformation and failure mode shearing along (100)/<010> can also be derived from the biaxial shear simulations as displayed in Fig. 5(a)–(d). The structural changes are clearly observed view along [010] direction. Fig. 5(a) displays the intact structure. With the shear strain increasing to 0.061, the Ga3–O7 (Ga_I–O_{III} type) bond bends to the (100) plane with the angle α to the (100) plane decreasing from original 31.2° to 14.3° because of the compressive stress. The Ga3–O7 bond distance slight increases from original 1.916 to 1.950 Å. This bond

rearrangement releases the shear stress from 2.4 GPa at 0.04 strain to 0.4 GPa at 0.061 strain. However, the total structure does not deconstruct because no bond is broken, as shown in Fig. 5(b). As the shear strain continuously increases to 0.187 which corresponds to maximum shear stress of 6.4 GPa, the Ga3-O7 bond increases from 1.95 to 2.15 Å and a new Ga3-O2 bond forms with bond distance of 1.94 Å, as shown in Fig. 5(c). Finally, the Ga3-O7 bond breaks, leading to the mechanical failure of the whole system (Fig. 5(d)) as the shear strain increases to 0.209. It is interesting to notice that the breaking of Ga_I-O_{III} bond leads to the failure of β -Ga₂O₃ under this particular slip system.

3.4 General stacking faults energy of β -Ga₂O₃

Dislocations, which are one-dimensional topological defects, are central to the understanding of mechanical properties of crystalline solids. The creation and motion of dislocations mediate the plastic response of a crystal to external stress. The dislocation core structure controls the mobility of dislocations, which accounts for the intrinsic ductility or brittleness of solids. To examine the dislocation core properties of β -Ga₂O₃, we computed the general stacking faults energy surface (γ -surface) of β -Ga₂O₃ along (001) slip plane. Previous experiments [49] suggested that the (001) and (100) plane are easy cleavage plane for β -Ga₂O₃. The above pure and biaxial shear deformation indicates that (001) plane is the most plausible slip plane. Therefore, we focus on the (001) plane γ -surface calculations.

We constructed a slab model with two unit cells along [001] direction, as shown in Fig. 6(a). The surface Ga and O atoms are terminated by H atoms to avoid the surface dangling bonds. To

obtain the optimized geometry, we first fixed the all the Ga and O atoms and only relaxed the H atoms in DFT simulation. Then all the atoms are relaxed to find optimized position before γ -surface calculation. Finally, the misfit energy across (001) plane is derived by displacing the upper half of the crystal (rectangular region in Fig. 6(a)). .

Fig. 6(b) displayed the γ -surface for (001) plane of β -Ga₂O₃. The structure at (0.5,0.5) corresponds to the only local minimum in the γ -surface. A close examination on this structure shows that this structure is actually the original crystalline structure. This is consistent with the *C2/m* symmetry of crystalline β -Ga₂O₃. Therefore, the β -Ga₂O₃ has no intrinsic stacking fault structure along the most plausible slip plane. In addition, the energy barrier of slipping along $\langle 010 \rangle$ is much lower than that along $\langle 100 \rangle$ direction, suggesting that the ideal shear strength along $\langle 010 \rangle$ direction is lower than that along $\langle 100 \rangle$ direction. This is consistent with the above ideal shear deformations.

We observed that there is no intrinsic stacking fault structure shear along (001) surface. However, previous experiments observed the screw dislocations lying on (201) and (001) planes with the Burgers vector parallel to [010] directions [50]. In addition, stacking faults, twinning and dislocation were observed in the nanoindentation experiments [48]. This suggests that dislocations may nucleate from different deformation mechanisms. In theory, the dislocation in homogenous system (such as single crystal) can initiate at the local nucleation sites which arise from the strain heterogeneities developed from mechanical local instabilities [58]. These instabilities can be developed under inhomogeneous deformation, occurring at lower local

stresses than those from ideal shear strength [58]. This provides possible paths for the dislocation nucleation in β -Ga₂O₃.

4. Summary

In summary, we used QM to examine the mechanical properties and intrinsic failure mechanisms of β -Ga₂O₃ under both pure shear and indentation stress conditions. Various plausible slip systems have been examined.

- We found that (001)/<010> slip system has the lowest ideal shear stress under pure shear deformation, which suggests it is the most plausible activated slip system. The failure mechanism for this slip system arises from breaking the Ga_{II}-O_{III} bond which is the weakest bond in β -Ga₂O₃.
- For indentation stress conditions, the (001)/<010> slip system is also the most plausible activated slip systems. The failure mechanism is the same as the pure shear deformation although it is highly compressive under indentation stress conditions.

We computed the unrelaxed γ -surface for β -Ga₂O₃ along (001) plane which is the most plausible slip plane. No local energy minimum is found in the γ -surface, suggesting that there is no intrinsic stacking fault structure for β -Ga₂O₃. Future studies are required to determine whether the β -Ga₂O₃ is brittle or ductile.

Acknowledgement

This work was supported by the NRC-HQ-84-15-G-0028 from Nuclear Regulatory

Commission (NRC) and National Science Foundation (CMMI-1727428). The simulations were performed on the high performance computing system at the University of Nevada, Reno.

References

- [1] S. I. Stepanov, V. I. Nikolaev, V. E. Bougrov, and A. E. Romanov, *Rev. Adv. Mater. Sci.* **44**, 63 (2016).
- [2] K. Nomura, H. Ohta, K. Ueda, T. Kamiya, M. Hirano, and H. Hosono, *Science* **300**, 1269 (2003).
- [3] J. F. Wager, *Science* **300**, 1245 (2003).
- [4] K. Nomura, H. Ohta, A. Takagi, T. Kamiya, M. Hirano, and H. Hosono, *Nature* **432**, 488 (2004).
- [5] R. Roy, V. G. Hill, and E. F. Osborn, *J. Am. Chem. Soc.* **74**, 719 (1952).
- [6] N. Ueda, H. Hosono, R. Waseda, and H. Kawazoe, *Appl. Phys. Lett.* **71**, 933 (1997).
- [7] M. Yamaga, T. Ishikawa, M. Yoshida, T. Hasegawa, E. G. Villora, and K. Shimamura, *Phys. Status Solidi C* **8**, 2621 (2011).
- [8] M. Higashiwaki, K. Sasaki, A. Kuramata, T. Masui, and S. Yamakoshi, *Appl. Phys. Lett.* **100**, 013504 (2012).
- [9] N. Suzuki, S. Ohira, M. Tanaka, T. Sugawara, K. Nakajima, and T. Shishido, *Phys. Status Solidi C* **4**, 2310 (2007).
- [10] E. G. Villora, K. Shimamura, Y. Yoshikawa, T. Ujiie, and K. Aoki, *Appl. Phys. Lett.* **92**, 202120 (2008).
- [11] K. Sasaki, M. Higashiwaki, A. Kuramata, T. Masui, and S. Yamakoshi, *J. Cryst. Growth* **378**, 591 (2013).

- [12] M. Fleischer and H. Meixner, *Sens. Actuators, B* **4**, 437 (1991).
- [13] M. Orita, H. Ohta, and M. Hirano, *Appl. Phys. Lett.* **77**, 4166 (2000).
- [14] B. J. Baliga, *IEEE Electron Device Lett.* **10**, 455 (1989).
- [15] K. Irscher, Z. Galazka, M. Pietsch, R. Uecker, and R. Fornari, *J. Appl. Phys.* **110**, 063720 (2011).
- [16] N. Ueda, H. Hosono, R. Waseda, and H. Kawazoe, *Appl. Phys. Lett.* **70**, 3561 (1997).
- [17] H. Aida, K. Nishiguchi, H. Takeda, N. Aota, K. Sunakawa, and Y. Yaguchi, *Jpn. J. Appl. Phys.* **47**, 8506 (2008).
- [18] K. Sasaki, A. Kuramata, T. Masui, E. G. Villora, K. Shimamura, and S. Yamakoshi, *Appl. Phys. Express* **5**, 035502 (2012).
- [19] H. Murakami, K. Nomura, K. Goto, K. Sasaki, K. Kawata, Q. T. Thieu, R. Togashi, Y. Kumagai, M. Higashiwaki, A. Kuramata, *et. al.*, *Appl. Phys. Express* **8**, 015503 (2015).
- [20] M. H. Wong, K. Sasaki, A. Kuramata, S. Yamakoshi, and M. Higashiwaki, *IEEE Electron Device Lett.* **37**, 212 (2016).
- [21] K. Sasaki, M. Higashiwaki, A. Kuramata, T. Masui, and S. Yamakoshi, *IEEE Electron Device Lett.* **34**, 493 (2013).
- [22] M. F. Yu, M. Z. Atashbar, and X. L. Chen, *IEEE Sens. J.* **5**, 1 (2005).
- [23] G. Kresse and J. Hafner, *Phys. Rev. B* **47**, 558 (1993).

- [24] G. Kresse and J. Furthmuller, *Comput. Mater. Sci.* **6**, 15 (1996).
- [25] G. Kresse and J. Furthmüller, *Phys. Rev. B* **16**, 11169 (1996).
- [26] G. Kresse and D. Joubert, *Phys. Rev. B* **59**, 1758 (1999).
- [27] Peter E. Blöchl, O. Jepsen, and O. K. Andersen, *Phys. Rev. B* **49**, 16223 (1994).
- [28] Y. Le Page and P. Saxe, *Phys. Rev. B* **65**, 104104 (2002).
- [29] R. Hill, *Proc. Phys. Soc. A*, **65**, 349 (1952).
- [30] D. Roundy, C. R. Krenn, M. L. Cohen, and J. W. Morris Jr., *Phys. Rev. Lett.* **82**, 2713 (1999).
- [31] B. Li, H. Sun, and C. F. Chen, *Nat. Commun.* **5**, 4965 (2014).
- [32] V. Vitek, *Philos. Mag.* **18**, 773 (1968).
- [33] S. Geller, *J. Chem. Phys.* **33**, 676 (1960).
- [34] S. Yoshioka, H. Hayashi, A. Kuwabara, F. Oba, K. Matsunaga, and I. Tanaka, *J. Phys. Condens. Matter* **19**, 346211 (2007).
- [35] S. F. Pugh, *Philos. Mag.* **45**, 823 (1954).
- [36] X. Q. Chen, H. Y. Niu, D. Z. Li, and Y. Y. Li, *Intermetallics* **19**, 1275 (2011).
- [37] A. O. Lyakhov and A. R. Oganov, *Phys. Rev. B* **84**, 092103 (2011)
- [38] A. Kelly and N. H. Macmillian, *Strong Solids*, 3rd ed. (Clarendon Press: Oxford, 1986).
- [39] F. Liu, P. B. Ming, and J. Li, *Phys. Rev. B* **76**, 064120 (2007).

- [40] S. Ogata, J. Li, and S. Yip, *Science* **298**, 807 (2002).
- [41] M. Jahnátek, J. Hafner, and M. Krajčí, *Phys. Rev. B* **79**, 224103 (2009).
- [42] Q. An, W. A. Goddard III, and T. Cheng, *Phys. Rev. Lett.* **113**, 095501 (2014).
- [43] Q. An and W. A. Goddard III, *Phys. Rev. Lett.* **115**, 105501 (2015).
- [44] G. D. Li, Q. An, W. A. Goddard III, P. C. Zhai, Q. J. Zhang, and G. J. Snyder, *Acta Mater.* **103**, 775 (2016).
- [45] M. de Jong, I. Winter, D. C. Chrzan, and M. Asta, *Phys. Rev. B* **96**, 014105 (2017).
- [46] I. S. Winter, M. de Jong, M. Asta, and D. C. Chrzan, *Phys. Rev. Materials* **1**, 030601(R) (2017).
- [47] C. M. Kube and M. de Jong, *J. Appl. Phys.* **120**, 165105 (2016).
- [48] Y. Q. Wu, S. Gao, and H. Huang, *Mater. Sci. Semicond. Process.* **71**, 321 (2017).
- [49] E. G. Villora, K. Shimamura, Y. Yoshikawa, K. Aoki, and N. Ichinose, *J. Cryst. Growth* **270**, 420 (2004).
- [50] K. Nakai, T. Nagai, K. Noami, and T. Futagi, *Jpn. J. Appl. Phys.* **54**, 051103 (2015).
- [51] A. Gouldstone, H. J. Koh, K. Y. Zeng, A. E. Giannakopoulos, and S. Suresh, *Acta Mater.* **48**, 2277 (2000).
- [52] G. S. Smith, E. B. Tadmor, and E. Kaxiras, *Phys. Rev. Lett.* **84**, 1260 (2000).
- [53] M. W. Barsoum, A. Murugaiah, S. R. Kalidindi, and T. Zhen. *Phys. Rev. Lett.* **92**, 255508 (2004).
- [54] Q. Huang, D. L. Yu, B. Xu, W. T. Hu, Y. M. Ma, Y. B. Wang, Z. S. Zhao, B. Wen, J.

- L. He, Z. Y. Liu, and Y. J. Tian, *Nature* **510**, 250 (2014).
- [55] E. B. Tadmor, R. Miller, R. Phillips, and M. Ortiz, *J. Mater. Res.* **14**, 2233 (1999).
- [56] S. Suresh and A. E. Giannakopoulos, *Acta Mater.* **46**, 5755 (1998).
- [57] B. Li, H. Sun, and C. F. Chen, *Phys. Rev. Lett.* **117**, 116103 (2016).
- [58] J. Li, T. Zhu, S. Yip, K. J. V. Vliet, S. Suresh, *Mater. Sci. Eng., A* **365**, 25 (2004).

Figure 1

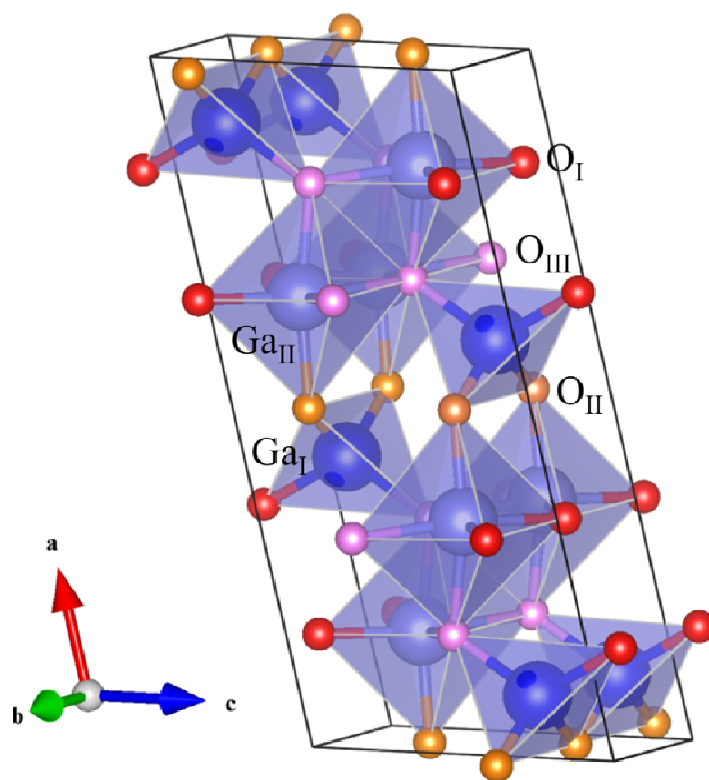


Figure 1. The β - Ga_2O_3 crystalline structures showing the nonequivalent Ga atoms and O atoms. The tetrahedral Ga_I , octahedral Ga_II , threefold coordinated O_I , threefold coordinated O_II , and fourfold coordinated O_III atoms are represented by the blue, light blue, red, yellow, and pink balls, respectively.

Figure 2

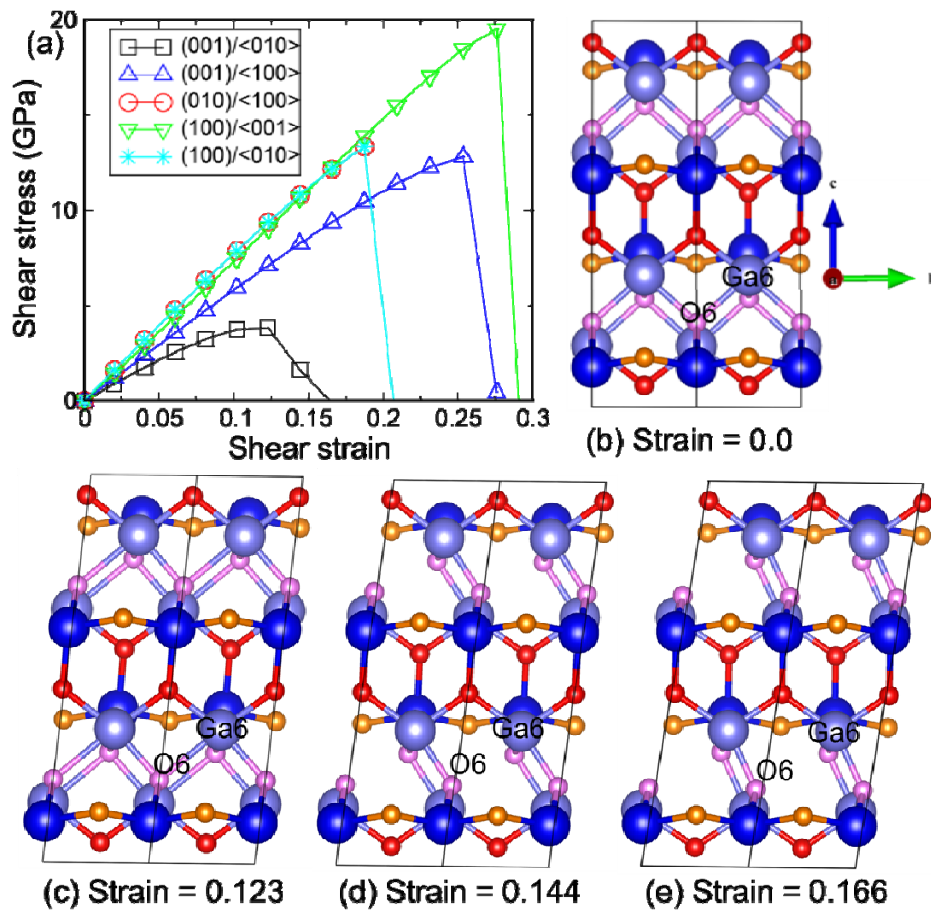


Figure 2. The shear-stress–shear-strain relationships of β -Ga₂O₃ shearing along various slip systems and structural changes for shear along the (001)/<010> slip system: (a) stress–strain relationships; (b) intact structure; (c) structure at 0.123 strain corresponding to the maximum shear stress of 3.8 GPa; (d) strain at 0.144 strain after failure in which the Ga6–O6 bond breaks; (e) structure at 0.166 strain which further releases the shear stress to ~0 GPa.

Figure 3

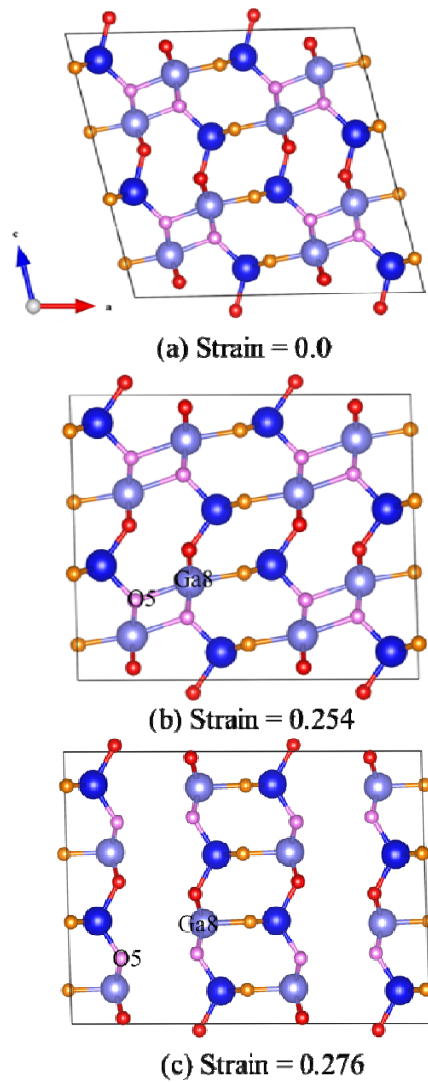


Figure 3. The structural changes of β - Ga_2O_3 in the failure process for shear along the (001)/ $\langle 100 \rangle$ slip system: (a) The intact structure; (b) The structure at 0.254 strain which corresponds to the maximum shear stress of 12.8 GPa; (c) Failed structure at 0.276 strain in which the Ga8-O5 bond breaks.

Figure 4

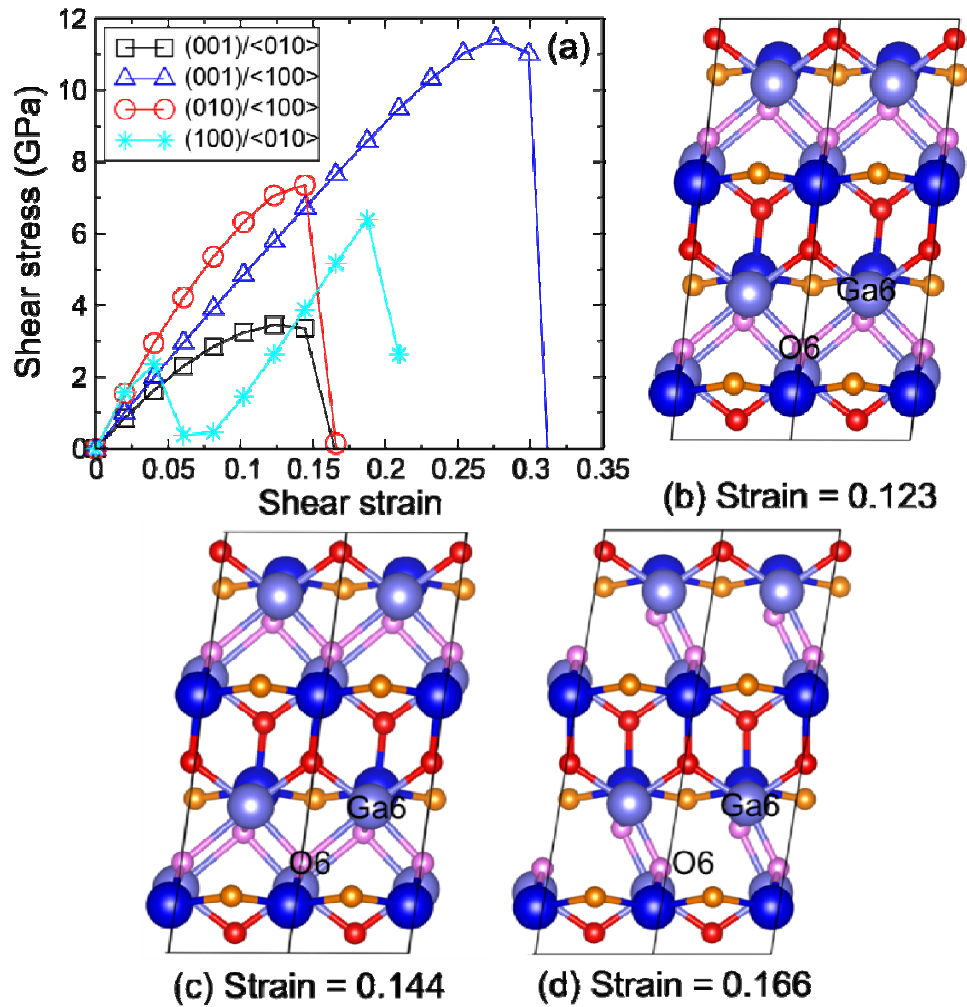


Figure 4. The shear-stress–shear-strain relationships and structural evolutions of β -Ga₂O₃ under indentation stress conditions for shear along the (001)/<010> slip system: (a) The shear-stress–shear-strain relationships; (b) structure at 0.123 strain corresponding to the maximum shear stress; (d) structure at 0.144 strain before failure; (e) structure at 0.166 strain after failure in which the Ga6–O6 bond breaks.

Figure 5

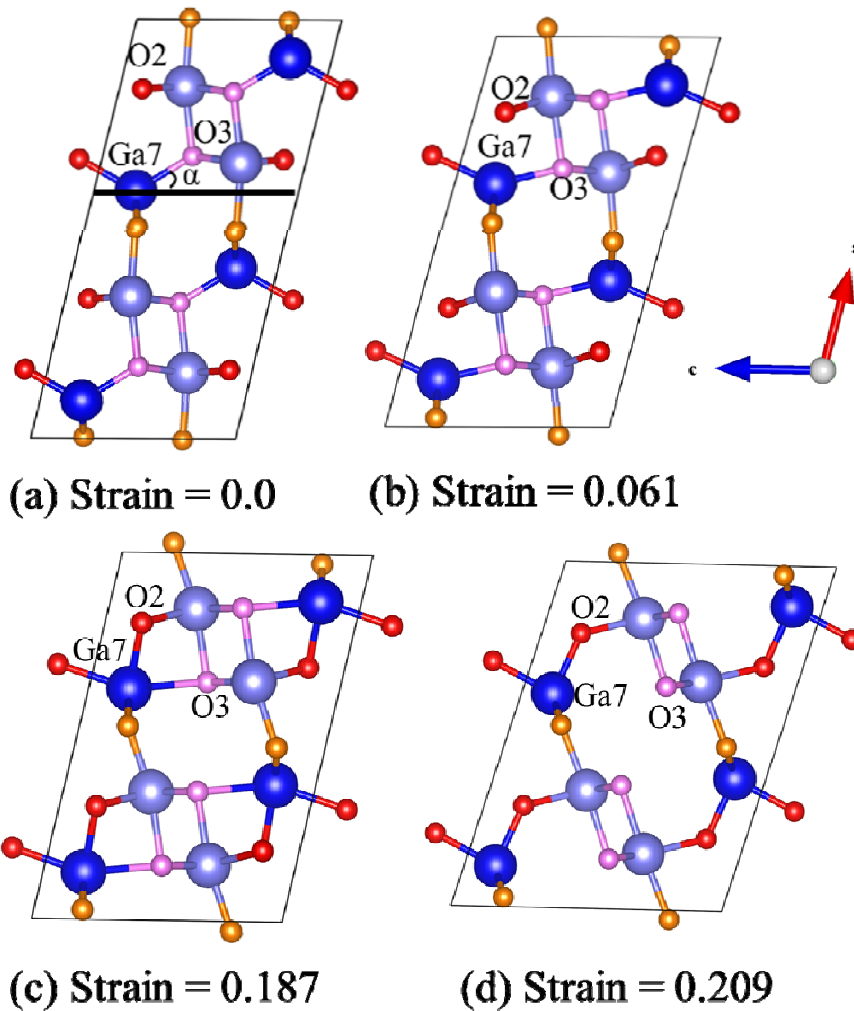


Figure 5. The structural evolutions of β -Ga₂O₃ under indentation stress conditions for shear along the (100)/ \langle 010 \rangle slip system: (a) intact structure; (b) structure at 0.061 strain corresponding to the 1st shear stress drop; (c) structure at 0.187 strain before failure; (d) structure at 0.209 strain after failure in which the Ga7–O3 bond breaks. Although the system is sheared along the \langle 010 \rangle direction, the structure changes are viewed along [010] direction for better visualization.

Figure 6

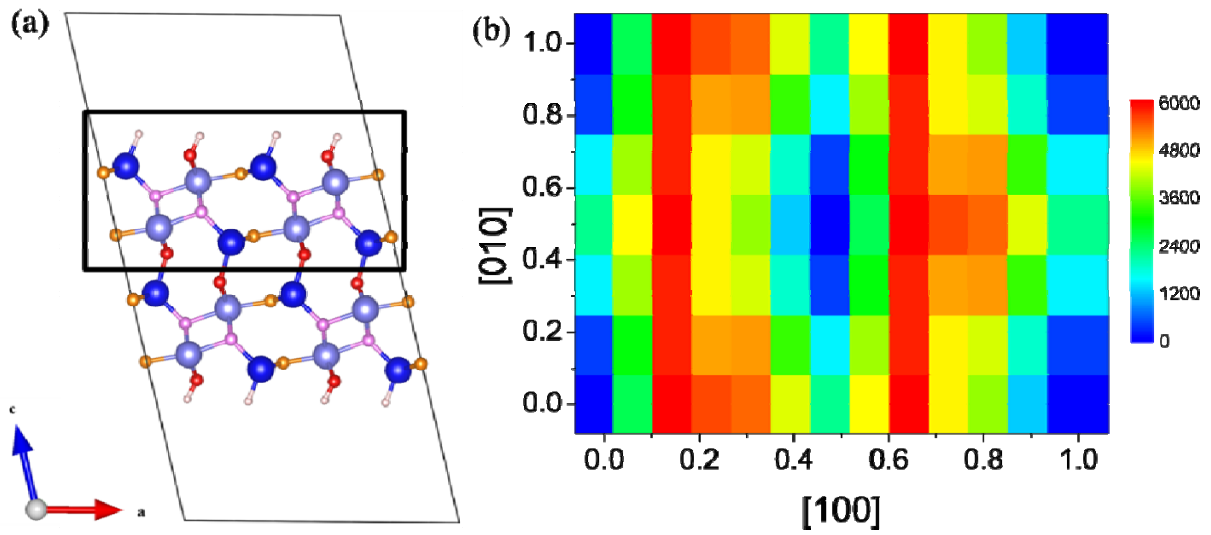


Figure 6. Unrelaxed γ -surface for β - Ga_2O_3 along the most plausible slip plane of (001) plane: (a) computation model to calculate γ -surface in which the surface Ga and O atoms are terminated by H atoms (white balls). The shifted upper unit cell is within rectangular region; (b) the unreaxed γ -surface (units: mJ/m^2) from DFT. The structure at (0.5,0.5) corresponds to the crystalline structure, which is consistent with $C2/m$ symmetry.